Control for powered-two wheeler stability assistance and autonomy: development of a test platform

Luca Bassani[1], James Fleming[2], Qusay Hawari[2], Stefano Lovato[1], Guitao Yang[2], Roberto Lot[1]
[1]*Università di Padova, Department of Industrial Engineering, 35131 Padua, Italy*
[2]*Wolfson School of Mechanical, Electrical and Manufacturing Engineering, Loughborough University, UK*

***Abstract*—Powered Two-Wheelers have complex lateral dynamics characterised by multiple modes (e.g. capsize, weave, and wobble) with natural frequencies, damping ratios and even stability properties that vary with forward speed of the vehicle. As such, they are a particularly challenging test case for path planning and lateral control. This work presents ongoing research on the control of roll and steer dynamics of a Fantic Issimo e-bike platform developed at the University of Padova. Specifically, we describe two baseline control architectures: a Proportional-Derivative (PD) controller and a Linear Quadratic Gaussian (LQG) controller. Both approaches utilise a Kalman-Bucy Filter for state estimation from the on-board Inertial Measurement Unit (IMU) and steering sensors. These results serve as a benchmark and platform validation in preparation for the future implementation of Linear Parameter-Varying Model Predictive Control (LPV-MPC) techniques, which will be necessary for robust constrained control of the highly speed-dependent motorcycle dynamics.**

***Index Terms*—Powered Two-Wheelers, Vehicle Dynamics, Stability Control, LQG Control, Autonomous Vehicles.**

I. Introduction

Accurate understanding and control of powered-two wheeled vehicle dynamics is crucial for the next generation of Advanced Rider Assistance Systems (ARAS). While the automotive sector has seen a rapid proliferation of active safety features—such as lane keeping and emergency braking, the implementation of equivalent systems for powered two-wheelers remains in its infancy [1]. This is despite the fact that powered two-wheelers are disproportionately represented in road accident statistics, with riders facing significantly higher fatality risks per mile travelled compared to car occupants [2].

Several technological solutions have been proposed for powered-two wheeled stability assistance. Gyroscopic stabilizers (GS), which use flywheels to generate righting moments, have proven effective in simulation studies [3], but they suffer from significant weight, cost, and power consumption penalties that limit their mass-market adoption. Alternatively, Steer-by-Wire (SbW) systems offer precise control [4] but sever the mechanical link between the handlebars and the wheel, raising safety and regulatory concerns. An alternative to both is active steering assistance, that applies an assistive torque to the steering column while maintaining a mechanical connection [5].

Research on autonomous and riderless bicycles has long focused on the problem of stabilizing inherently unstable single-track vehicles. Early experimental efforts were carried out in highly controlled environments, typically using rollers or treadmills. Tanaka and Murakami [6] demonstrated one of the first self-stabilizing bicycle robots, validating a steering-based controller through simulations and experiments on a roller, with the primary goal of maintaining upright equilibrium around 0 deg roll. Similarly, Shafiekhani et al. [7] evaluated an adaptive neuro-fuzzy controller on a treadmill, again targeting stabilization at 0 deg roll without examining the stability characteristics of the bicycle across different forward velocities. Andersson et al. [8] adopted a loop-shaping strategy to tune a PID steering controller and validated it on a roller at a fixed speed of 14 km/h, yet without providing a broader analysis of velocity-dependent stability. Subsequent studies moved beyond roller-based testing, performing experiments on free-running prototypes, yet still focusing on tracking a zero-roll equilibrium. Cerone et al. [9] proposed an LPV controller and, importantly, provided an explicit analysis of the speed-dependent instability of the bicycle, highlighting qualitatively different dynamic regimes. Their experiments were deliberately conducted at very low speeds (1.0–1.7 m/s) in coast-down, i.e., well within the open-loop unstable region of the vehicle, while still aiming to regulate roll toward 0 deg under LPV state feedback. Baquero-Suárez et al. [10] employed an Active Disturbance Rejection Control (ADRC) architecture and validated their design on both multibody simulations and physical experiments, showing that the system could maintain upright balance at constant velocities between 1.5 and 2.35 m/s, with additional modeling discussion on non-minimum-phase behavior below 0.78 m/s and self-stable behavior above 3.15 m/s. Smith et al. [11] implemented an LPV-inspired gain-scheduled PID controller for a bicycle actuated via linear electric steering actuators; their tests consisted of manually pushing the bicycle to 3–4 m/s and observing coast-down behavior during which the controller maintained upright equilibrium, without analyzing how stability changed with speed variations. Xiangrun et al. [12] addressed low-speed stabilization for an inertia-wheel-based auto-balancing bicycle using a Linear Extended State Observer to reject disturbances and uncertainties. Their objective remained the regulation of the bicycle states toward the upright configuration, with experiments confirming stabilization accuracy on the order of 0.4 deg despite perturbations, but again without studying velocity-dependent stability properties. More recently, research has also explored stabilization at non-zero roll angles, enabling maneuvering rather than mere upright balancing. Wang et al. [13] developed a cascaded

Proportional-Derivative (PD) control scheme for both balance and directional control at approximately 5 m/s, where the inner loop stabilizes the roll angle toward a reference that may be non-zero—thus enabling curved trajectories—while the outer loop regulates yaw angle to generate the corresponding roll reference. Beyond stabilization, Gabriel et al. [14] introduced one of the most advanced implementations to date, combining Optimal Preview Control with quintic-polynomial pursuit for full path-tracking control. Their architecture enables stabilization and accurate tracking of complex paths, including tight turns, operating at low speeds (≈ 2 m/s) and addressing practical steering limitations. In this case, the experimental campaign was conducted in a controlled indoor environment—specifically within an office-building setting—and no analysis of the vehicle's stability was carried out.

Compared to previous studies, the novelty of this work lies in the experimental validation of steering-based stabilization and cornering control on a free-running, rider-capable powered two-wheeler operating in speed regimes that are inherently unstable. The proposed approach combines outdoor experimental testing with a velocity-domain stability analysis conducted below the natural self-stability threshold of the vehicle, while demonstrating controlled regulation both around the upright condition and at non-zero roll angles during cornering maneuvers. These elements are addressed within a unified experimental framework, providing a realistic and systematic testbed for the development and future validation of advanced LPV model predictive control strategies. In the present work, this framework is employed to test model-based steering assistance controllers on the Self-Balancing Bike (SBB) platform at the University of Padova. As a preliminary step toward constrained LPV-MPC design [15], baseline PD and LQG control architectures, together with a Kalman-Bucy filter for state estimation, are implemented and experimentally evaluated.

The structure of the paper is as follows: Section II describes the experimental platform used for this work. Section III presents the dynamic model adopted, the control strategies implemented, the roll-angle estimation method based on a Kalman filter and the speed analysis. Section IV describes the tests performed. Finally, Section V reports and discusses the results obtained from the experimental tests.

II. Platform

The Self-Balancing Bike (SBB) test platform is a modified Fantic Issimo Urban e-bike (36 kg) equipped with a 250 W pedal-assist motor (Fig. 1). Steering is actuated by a Maxon EC45 brushless DC motor (70 W, 24 V) coupled with a Maxon GP42C planetary gearhead (36:1) and connected to the steering shaft via a 1.25:1 belt transmission. This setup provides a peak assistive steering torque of 14 Nm while preserving a mechanical connection for safety. To support state estimation and control, the platform is equipped with sensors including an Inertial Measurement Unit (IMU), GPS, wheel speed encoders, steering potentiometers, and a custom-calibrated torque sensor on the handlebars (see Table I). A secured system was implemented on the bike to prevent the vehicle to roll over during autonomous stop after completing the test maneuver. Data acquisition and control loop execution (running at 1 kHz) are handled by an onboard Teensy 4.1 microcontroller, for which code may be generated from Simulink for rapid prototyping. For model-based control design iterations, the Simulink files can also be used for co-simulation with the motorcycle Simulation software FastBike [16] before deploying to the SBB hardware.

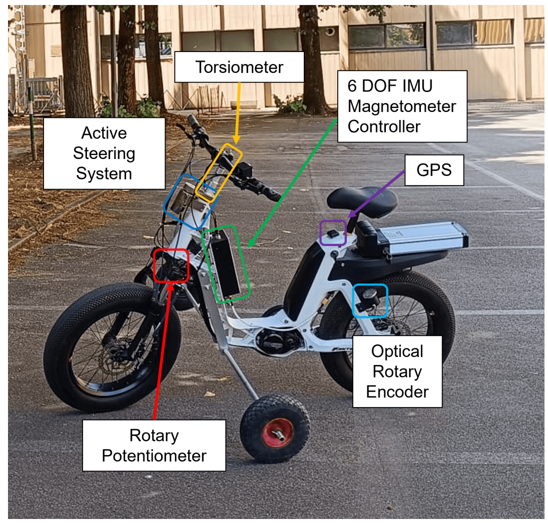

Fig. 1. Self Balancing Fantic Issimo Urban e-bike for this project.

III. Estimation and control design

To achieve robust stabilization, a model-based control approach was adopted, supported by a state estimation layer to handle sensor noise. For control design, a nonlinear multibody model of the bike was linearised in straight running conditions, leading to a linear system in descriptor state space form as:

$$E\dot{x} = Ax + Bu \tag{1}$$
$$x = [v_y \ \dot{\psi} \ \dot{\theta} \ \dot{\delta} \ \dot{\phi} \ \alpha_r \ \alpha_f \ \theta \ \delta \ \phi]$$

where v_y is the lateral speed, $\theta,\ \delta,\ \phi,\ \dot{\theta},\ \dot{\delta},\ \dot{\phi}$ are the roll, steering, and rider leaning angles, and their rates, respectively. $\dot{\psi}$ is the yaw rate, $\alpha_r,\ \alpha_f$ are the rear and front tyre sideslips, respectively. Typically, E is nonsingular but the descriptor form improves numerical conditioning when using (1). The bike layout is shown in Fig. 2 with model parameters defined in Table II. It is worth noting that some of the states within the state space are associated with the rider. This is because the model employed is a more general simulation-oriented framework that also accounts for rider-induced effects. In the context of the present study, the structure of the model was not altered; instead, all rider-related parameters were simply set to zero.

Knowing the current roll angle and roll rate of the bike is vital for stabilisation, however it cannot be measured directly. To estimate it and other states, a continuous-time Kalman-Bucy Filter (KBF) was designed to fuse data from the IMU

TABLE I
SENSORS CHARACTERISTICS.

Parameter	Sensor	Characteristics
Steer Angle	Rotary Potentiometer	Resistance: 3 kΩ; range: 100 deg
Speed	Rotary Optical Encoder	Counts per revolution: 100; 3 otput signals (A,B,Z)
GPS	Adafruit Ultimate GPS	Position accuracy: 1.8 m; update rate: 10 Hz
IMU	ISM330DHCX	a range: ± 19.6 m/s; ω range: ± 2000 deg/s; update rate: 3333 Hz
Magnetic field	LIS3MDL	Magnetic range: ± 4 G; update rate: 200 Hz

TABLE II
MODEL PARAMETERS USED.

Factor	Unit	Value	Description
m	[kg]	38.6	Bike mass
$(m_f,\ m_r)$	[kg]	(3.6, 5)	Front and rear tyre mass
w	[m]	1.149	Wheelbase
$(b,\ h)$	[m]	(0.483, 0.459)	Center of mass position of the Bike
r_0	[m]	0.295	Front and rear tyre radius
ρ	[m]	0.06	Tyre cross-sectional radius of curvature
a_n	[m]	0.08	Normal trail
β	[deg]	26.5	Caster angle
$(I_{zz},\ I_{xx},\ I_{xz}\ )$	[kg m^2]	(7.000, 2.520, 1.200)	Bike moments of inertia
I_{fzz}	[kg m^2]	0.12	Front principle moment of inertia
$(i_{fy},\ i_{ry})$	[kg m^2]	0.152	Front and rear wheel axial inertia
$(C_\lambda,\ C_\phi)$	[-]	(15, 0.94)	Front and rear tyre stiffness
$(Cf_a,\ Cr_a)$	[-]	-0.16	Self-aligning moment coefficients
$(Cf_t,\ Cr_t)$	[-]	0.02	Overturning moment coefficients
c_δ	[Nm/rad s^{-1}]	5	Steering column damping
$(K_{yf},\ K_{yr})$	[Nm/rad]	68000	Carcass stiffness
$(N_f,\ N_r)$	[-]	(279.01, 758.47)	Tyre relaxation parameters

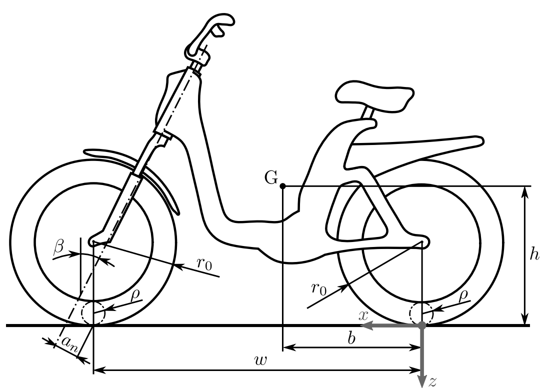

Fig. 2. Layout of the bike model. Table II summarize all the model variables.

and steering sensors. Specifically, the filter takes in three measurements: steer angle (δ), yaw rate ($\dot{\psi}$), and roll rate ($\dot{\theta}$), and estimates the full lateral dynamics state of the system.

Two distinct control strategies were implemented for testing. A classical PD controller was implemented to track a roll angle reference. The controller acts on the error between the estimated roll angle and the reference, calculating a requested steering torque. This mimics the natural counter-steering behavior of a human rider. An optimal Linear Quadratic Gaussian (LQG) controller was also tested, for which the state vector was augmented with an integral error state x_e. To respect the physical limits of the Maxon motor, a hard saturation block constrains the output torque to ± 14 Nm. Both controllers were tuned on the linearised model to achieve a robust phase margin of approximately 60 deg, which corresponds to closed-loop dynamics with a dominant damping ratio close to 70%, as verified from the loop-gain Bode plot inspection in Simulink.

A. Kalman Filter

The Kalman filter designed for estimating the unknown roll angle and other vehicle states based on chassis gyro and steer angle measurements, incorporating stochastic disturbance inputs, nonlinear effects in tyre forces, un-modelled drag or inertial forces is here presented. We may define an output equation for the state-space model as $y = Cx$, where the vector y contains the measurements of on-board sensors, i.e. the yaw and roll rates and steer angle. We then introduce a state observer that updates an estimate $\hat{x}$ of the vehicle state x as

$$E\dot{\hat{x}} = A(v)\hat{x} + Bu + L(v)[y - C\hat{x}] \tag{2}$$

in which feedback from the error in measured outputs is used to refine the estimate. In accordance with standard theory, for a fixed v the error $e = x - \hat{x}$ of this estimate will decay to zero if and only if the matrix $A(v) - L(v)C$ has eigenvalues in the left half of the complex plane.

To choose $L(v)$ for a given speed, we employ the steady-state gain of the Kalman-Bucy filter, as may be calculated in MATLAB using the 'kalman' function. To carry out the calculation of $L(v)$, we must specify covariances for any measurement and process noise. Interestingly, for good performance when applying the resulting filter to the bike, it is observed that the covariance of noise on the tyre forces must be specified as a factor of 100 larger than that of sensor and other state noise. This is likely due to a mismatch in the simplified tyre model assumed here and that used in the nonlinear simulation.

B. PD control formulation

The PD controller applies a negative feedback to the roll error and roll rate

$$u = -K_{pd}\left(e_\theta + T_d\dot{\hat{\theta}}\right) \quad (3)$$

where K_{pd}, T_d are parameters referred to as the gain and derivative time respectively and roll error $e_\theta = \theta - \hat{\theta}$ (see Fig.3). Note that unlike a classical PD controller that differentiates its input signal, this controller will have improved noise properties by exploiting the estimate of roll rate provided by the Kalman Filter.

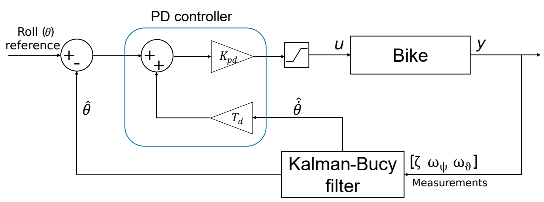

Fig. 3. Block diagram of PD + KF controller

C. LQ control formulation

The LQ control policy minimises the cost

$$J = \sum_{k=t}^{\infty}[qe_\theta^2 + q\dot{\hat{\theta}}^2 + ru^2] \quad (4)$$

where u is the steer torque control input, and r is a scalar control penalty, corresponding to the single control input in this system. Parameter q is a control weight for the roll error e_θ and roll rate $\dot{\theta}$ (see Fig. 4). The cost function in (4) is written in output form, i.e., C^TQ_oC, where Q_o is an output weighing square matrix. A more general cost function can be considered, such as a quadratic form of the states as x^TQx, although is less straightforward to tune as it contains 10 parameters for our application.

The design incorporates the integral of the roll error as a state, hence the appended state space system is:

$$\begin{bmatrix} x_{k+1} \\ x_{e_\theta k+1} \end{bmatrix} = \begin{bmatrix} A & 0 \\ T_sC_{e_\theta} & 1 \end{bmatrix}\begin{bmatrix} x_k \\ x_{e_\theta k} \end{bmatrix} + \begin{bmatrix} B \\ 0 \end{bmatrix} \quad (5)$$

where matrix C_{e_θ} is the section of the C matrix corresponding to the roll output and has dimensions 1×10.
The closed-loop dynamics are then

$$x_{k+1} = A_dx_k - BK\hat{x}_k \quad (6)$$

where $\hat{x}_k$ are the estimated states.

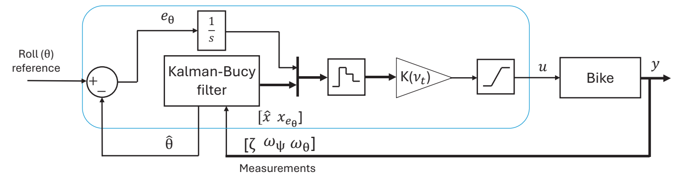

Fig. 4. Block diagram of LQ + KF controller

D. Speed analysis

To determine test speed, an open loop root-locus analysis of the linearized system model poles was performed. Fig. 5 illustrates how the most critical mode of the model evolves as a function of speed. This mode is used as the primary indicator for assessing the stability or instability characteristics of the vehicle. At low forward speed ($V_x = 2.5$ m/s), the capsize mode, a non-oscillatory mode associated with the roll-over dynamics of the vehicle, is unstable, as indicated by its poles lying in the right-half complex plane with zero imaginary part. As the forward speed increases, this mode becomes oscillatory and transitions into what is commonly referred to as the weave mode. At approximately $V_x = 5.9$ m/s, the system undergoes a stability transition: the real part of the weave mode crosses into the left-half plane, indicating that the mode becomes stable. Based on this analysis, the maximum test speed was set to $V_x = 2.5$ m/s, in order to evaluate the controllers within a highly unstable operating region of the vehicle.

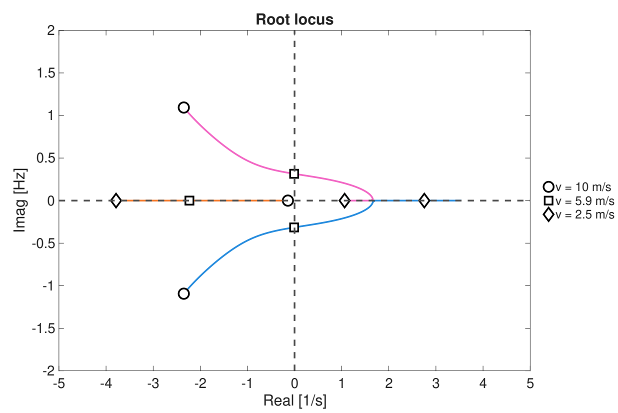

Fig. 5. Root locus of the linearized model as a function of forward speed, obtained by simulating the open-loop system from 1 m/s to 10 m/s. The capsize/weave mode, initially unstable, becomes stable at approximately 5.9 m/s.

IV. Test Description

Two types of tests were conducted: a straight-line run of approximately 30 m and a left-hand turn with a curvature radius of about 6 m, followed by a 15 m straight segment. All tests were carried out safely in a closed, obstacle-free asphalted outdoor parking area at the University of Padova, with no access to the public (Fig. 6). The forward velocity was kept constant throughout each trial. As summarized in Table III, for the cornering scenario, both the PD and the LQG controllers were tested. In this case, two forward velocities were selected: 2.5 m/s and 1.5 m/s. The use of both controllers in the turning maneuver allowed us to compare their performance in tracking a non-zero roll reference while executing a curve of fixed radius. Straight-line tests were carried out exclusively using the PD controller, which was evaluated at four different constant velocities: 2.5, 2.0, 1.5, and 1.0 m/s.

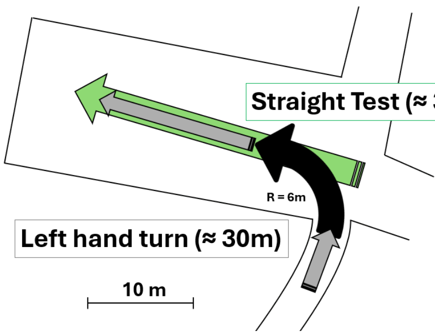

Fig. 6. Car park layout and test line followed during straight and left-hand turn Test.

TABLE III
SUMMARY OF THE EXPERIMENTAL TESTS.

Test type	Controller	Test speeds [m/s]
Left-hand turn	PD, LQG	2.5, 1.5
Straight-line	PD	2.5, 2.0, 1.5, 1.0

V. RESULTS AND CONCLUSION

Straight and cornering tests (Fig. 7) were performed, with the bike operating without a rider, following a roll reference. Fig. 8 illustrates cornering performance at 2.5 m/s with a fixed 6 deg roll reference. The experimental data indicates that the LQG controller is more active compared to the PD controller as seen in Fig.8. The LQG successfully suppresses oscillations when maintaining a fixed roll reference during cornering.

Low-speed cornering tests (1.5 m/s) were also performed, but both controllers failed to stabilize the vehicle under these conditions. At this very low forward velocity, given the fixed curvature radius of 6 m, the corresponding roll reference is close to zero (approximately 2.2 deg). This extremely small roll demand contributed to the inability of both controllers to successfully complete the maneuver. For straight-line maneuvers only the PD controller was evaluated at multiple forward velocities, ranging from 2.5 m/s down to very low speeds, comparable to normal walking speed, of 1 m/s, with decrements of 0.5 m/s. In all these scenarios, the controller successfully stabilized the vehicle around a roll angle of zero. Each experimental condition was repeated three times. Fig. 9–12 present the first trial conducted at each velocity. Table IV reports the root-mean-square error (RMSE), averaged across all three repetitions, for both the roll angle and the steering-torque current generated by the controller. It can be observed that at very low velocity (1 m/s) the controller had to exert more aggressive steering actions even reaching the saturation (Fig. 12) to counteract the natural capsize mode,

TABLE IV
PD CONTROLLER PERFORMANCE AT DIFFERENT SPEEDS IN A STRAIGHT LINE SCENARIO (AVERAGE OF THREE TESTS)

Speed [m/s]	Roll RMSE [deg]	Steer Current RMSE [A]
2.5	0.995	2.340
2.0	0.993	2.273
1.5	0.780	2.565
1.0	0.885	4.695

which becomes increasingly unstable at lower forward speeds. Consequently, future research will investigate the implementation of Model Predictive Control (MPC) to mitigate this demand by enforcing constraints on the steer current, steer and roll angles, while maintaining bike stability.

Fig. 7. Bike during cornering test.

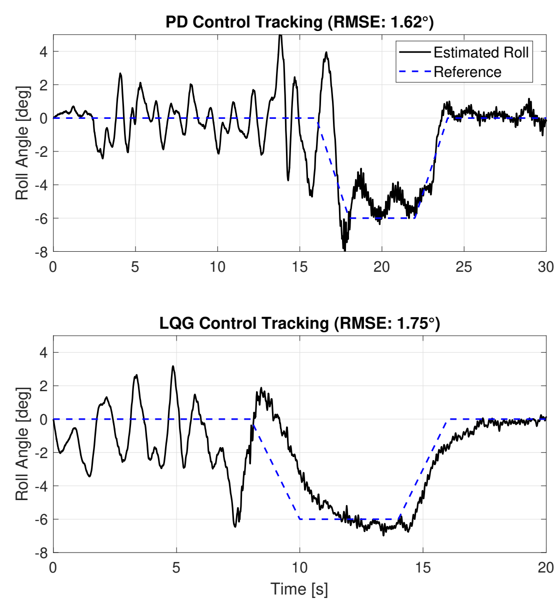

Fig. 8. Cornering scenario for PD and LQG controllers at 2.5m/s

REFERENCES

[1] G. Savino, M. Pierini, and M. Fitzharris, “Motorcycle active safety systems: Assessment of the function and applicability using a population-based crash data set,” *Traffic injury prevention*, vol. 20, no. 4, pp. 406–412, 2019.

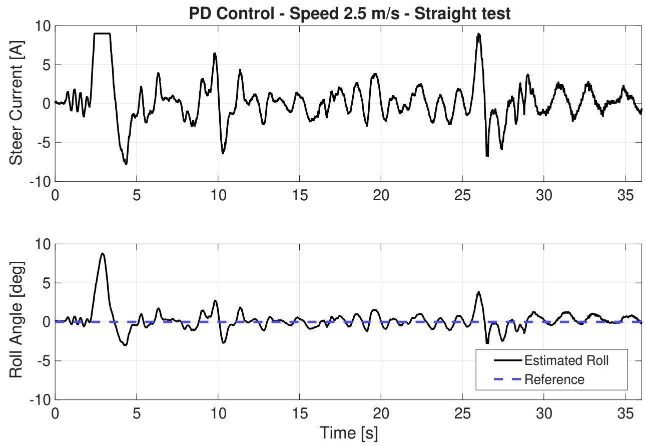

Fig. 9. PD controller - Straight Test 1 - 2.5 m/s. Steer current [A] and Roll Angle [deg] data.

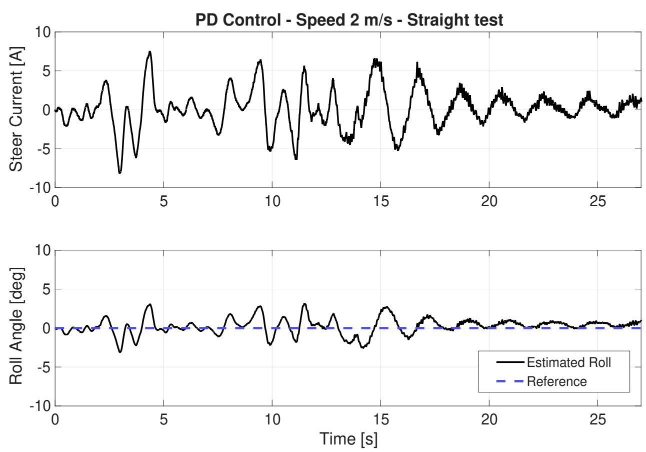

Fig. 10. PD controller - Straight Test 1 - 2 m/s. Steer current [A] and Roll Angle [deg] data.

[2] "Reported road casualties in great britain, provisional estimates: year ending june 2025," https://www.gov.uk/government/statistics/reported-road-casualties-in-great-britain-provisional-estimates-year-ending-june-2025/reported-road-casualties-in-great-britain-provisional-estimates-year-ending-june-2025casualties-by-road-user-type, [Accessed 13-02-2026].

[3] R. Lot and J. Fleming, "Gyroscopic stabilisers for powered two-wheeled vehicles," *Vehicle system dynamics*, 2019.

[4] Y. Marumo and M. Nagai, "Steering control of motorcycles using steer-by-wire system," *Vehicle System Dynamics*, vol. 45, no. 5, pp. 445–458, 2007.

[5] S. Lovato, M. Bova, M. Massaro, M. Andriollo, and R. Lot, "Active steering assistant for powered two-wheelers: Hardware prototyping and results," in *The International Conference of IFToMM ITALY*. Springer, 2022, pp. 361–369.

[6] Y. Tanaka and T. Murakami, "Self sustaining bicycle robot with steering controller," in *The 8th IEEE International Workshop on Advanced Motion Control, 2004. AMC'04.* IEEE, 2004, pp. 193–197.

[7] A. Shafiekhani, M. J. Mahjoob, and M. Akraminia, "Design and implementation of an adaptive critic-based neuro-fuzzy controller on an unmanned bicycle," *Mechatronics*, vol. 28, pp. 115–123, 2015.

[8] T. Andersson, N. Persson, A. Fattouh, and M. C. Ekström, "A loop shaping method for stabilising a riderless bicycle," in *2019 European Conference on Mobile Robots (ECMR)*. IEEE, 2019, pp. 1–6.

[9] V. Cerone, D. Andreo, M. Larsson, and D. Regruto, "Stabilization of a riderless bicycle [applications of control]," *IEEE Control Systems Magazine*, vol. 30, no. 5, pp. 23–32, 2010.

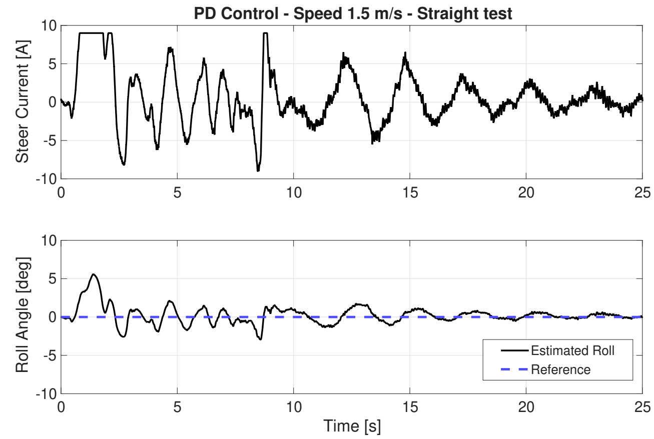

Fig. 11. PD controller - Straight Test 1 - 1.5 m/s. Steer current [A] and Roll Angle [deg] data.

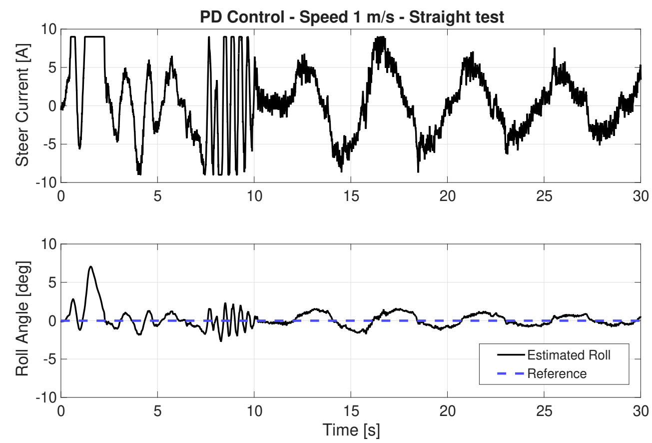

Fig. 12. PD controller - Straight Test 1 - 1.5 m/s. Steer current [A] and Roll Angle [deg] data.

[10] M. Baquero-Suárez, J. Cortés-Romero, J. Arcos-Legarda, and H. Coral-Enriquez, "A robust two-stage active disturbance rejection control for the stabilization of a riderless bicycle," *Multibody System Dynamics*, vol. 45, no. 1, pp. 7–35, 2019.

[11] R. Smith, Z. Fawaz, A. Mohammadi, P. Muench, and S. Lakshmanan, "Linear parameter varying-based control of a riderless bicycle with linear actuators," in *Unmanned Systems Technology XXI*, vol. 11021. SPIE, 2019, pp. 66–72.

[12] D. Xiangrun, T. Panlong, and Z. Xiaoyu, "Stabilization control of auto-balancing bicycle subject to disturbances," in *2023 35th Chinese Control and Decision Conference (CCDC)*. IEEE, 2023, pp. 1551–1556.

[13] L. X. Wang, J. M. Eklund, and V. Bhalla, "Simulation & road test results on balance and directional control of an autonomous bicycle," in *2012 25th IEEE Canadian Conference on Electrical and Computer Engineering (CCECE)*. IEEE, 2012, pp. 1–5.

[14] D. Gabriel, D. Görges, and D. Baumgärtner, "On the development of a path tracking controller by combining optimal preview control and pursuit control methods," in *The Evolving Scholar-BMD 2023, 5th Edition*, 2024.

[15] J. Fleming and Q. Hawari, "Robust tube mpc using gain-scheduled policies for a class of LPV systems," *IEEE Control Systems Letters*, vol. 8, pp. 1589–1594, 2024.

[16] "FastBike software, Dynamotion – dynamotion.it," https://www.dynamotion.it/en/software/fastbike-software/, [Accessed 13-02-2026].